Electric field splitting of the octatetraene 11 A g →21 A g transition in n-hexane

Gerhard Gradl, Bryan E. Kohler, and Curtis Westerfield

Citation: The Journal of Chemical Physics **97**, 6064 (1992); doi: 10.1063/1.463717
View online: http://dx.doi.org/10.1063/1.463717
View Table of Contents: http://scitation.aip.org/content/aip/journal/jcp/97/9?ver=pdfcov
Published by the AIP Publishing

Electric field splitting of the octatetraene 1 $^1A_g \rightarrow 2\ ^1A_g$ transition in *n*-hexane

Gerhard Gradl, Bryan E. Kohler, and Curtis Westerfield
Department of Chemistry, University of California, Riverside, California 92521-0403

(Received 23 June 1992; accepted 31 July 1992)

Octatetraene can be photoisomerized even when it is incorporated in a low temperature *n*-hexane crystal. When this is done by irradiating the zero-phonon component of the $S_0 \rightarrow S_1$ origin band with a single frequency laser, very narrow ($\sim$10 MHz) persistent holes can be burned. We have determined the effect of an externally applied electric field on these persistent holes and fit the observed data with a simple quantum mechanical model parameterized in the $S_0 \rightarrow S_2$ and $S_1 \rightarrow S_2$ transition dipoles and the magnitude of a molecular field intrinsic to the *n*-hexane site occupied by the octatetraene guest. The magnitude of the molecular field ($\sim 10^6$ V/cm) is consistent with only one of the three possible *n*-hexane sites that could have accommodated the octatetraene guest.

I. INTRODUCTION

Given the enormous increase in resolution that can be realized in hole burning studies, the application of these techniques to determine the spectroscopic consequences of applied electric fields was a natural extension.[1–13] To date most of the experiments have addressed organic chromophores in optically transparent glasses or polymer films, an important exception being the measurements on free-base chlorin in single crystals of *n*-hexane and *n*-octane by Dicker, Johnson, Noort, and van der Waals.[2]

Three aspects of linear polyene electronic structure make electric field effect experiments on these molecules especially informative. First, these molecules are intrinsically nonpolar. Of course, in the centrosymmetric all-*trans* conformation symmetry requires that the isolated molecule have no permanent dipole moment. However, noncentrosymmetric isomers are also expected to have vanishingly small diagonal dipole moment matrix elements because of the charge neutrality of the carbon skeleton. This charge neutrality is expected from simple molecular orbital or band theoretical considerations, and it is also found in more elaborate theoretical treatments.[14] Because of Hückel pairing symmetry (identical magnitudes of atomic orbital coefficients for bonding and antibonding molecular orbitals—this is also called electron-hole symmetry) the ground 1 ^1A_g and second excited 1 ^1B_u singlet state [highest occupied molecular orbital (HOMO) to the lowest unoccupied molecular orbital (LUMO) excitation from the ground configuration] are completely charge neutral. This is also the case for the first excited 2 ^1A_g singlet state insofar as it is described as a mixture of the HOMO to LUMO double excitation with the symmetric linear combination of the HOMO to LUMO+1 and HOMO−1 to LUMO configurations. This level of description of polyene electronic structure has been shown to reproduce accurately the S_1 and S_2 excitation energies of all linear polyenes.[15]

Second, the gap between S_1 and S_2 is relatively small (3500 cm^{-1} for all-*trans* octatetraene in *n*-hexane) and the off-diagonal dipole moment matrix element is symmetry allowed and relatively large.[16] The observed vibronic development of the spectra are consistent with the idea that the Franck–Condon factors for the mixing of higher lying 1 ^1B_u levels will only be significant for the C=C double bond stretch vibrations, whose frequency is half that of the electronic gap. This means that, with respect to hole burning studies on the 1 ^1A_g to 2 ^1A_g origin, the primary effect of an applied electric field is to mix the 2 ^1A_g and 1 ^1B_u zero point levels. Thus, it is reasonable to treat the data in terms of a two level model with a known energy gap parameterized in the local field and the 2 ^1A_g–1 ^1B_u transition dipole.

Third, because of the long lifetime of the excited 2 ^1A_g state, the intrinsic hole width is extremely narrow [3.2 MHz half-width at half-maximum (HWHM) for octatetraene in *n*-hexane[17]]. This means that the effects of applied electric fields can be registered with very high resolution, which removes ambiguity from the interpretation of the observed effects.

This paper reports studies of the effects of applied electric fields on photochemical holes burned into the 1 $^1A_g \rightarrow 2\ ^1A_g$ 0–0 transition of *trans,trans*-octatetraene in randomly oriented microcrystals of *n*-hexane. Because the sample consists of nonpolar molecules in a well defined site in the host lattice, one might have expected a second order Stark shift which, given the random orientation of the applied field in the octatetraene axis system, would have simply caused the hole to asymmetrically broaden to lower energy with the application of an external electric field. In fact, the photochemical hole splits in a way that is accurately modeled by assuming that the octatetraene molecules experienced the vector sum of the applied field and a large well defined internal field oriented in the molecular axis system. This field is reasonably accounted for by summing the electric fields of the *n*-hexane C–H bond dipoles over the crystal lattice for one of three possibilities for the guest site. The large magnitude of this internal field and the fact that, to within the resolution of our experiments, its effective projection on the octratetraene 2 $^1A_g \rightarrow 1\ ^1B_u$ transition dipole is the same for all molecules in the ensemble has important implications. For example, once one realizes that even in nonpolar materials environmental asymmetry can generate local fields in the 10^6 V/cm range, it becomes

 0021-9606/92/216064-08$06.00

very important to take this into consideration when discussing charge generation and separation. It is quite reasonable to propose that the electrostatic field of the asymmetric protein environment of the photosynthetic unit is responsible for the unidirectional electron transfer rather than any subtle property of the special pair.

II. EXPERIMENT

Octatetraene was synthesized using the method described by Spangler and Little[18] and stored in *n*-pentane solution at $-10\,^{\circ}C$. In time, the absorption spectrum of this stock solution showed evidence of an impurity absorbing at shorter wavelengths than octatetraene. This was removed by classical chromatography on a 20 cm long by 1 cm diam alumina column, eluting with spectra-grade hexanes. The purified octatetraene was then transferred to *n*-hexane by injecting $\sim 50\ \mu\ell$ of the eluent from the alumina column into an high pressure liquid chromatograph (HPLC) (Waters U6K injector with Waters model 6000A solvent delivery system) where the *n*-hexane constituted the mobile phase. Although the column used (Hibar Lichrosorb Si60 5 μ) did not separate *cis,trans* and *trans,trans* octatetraene, it did separate the octatetraene from the hexanes with minimal dilution. The eluting octatetraene was detected by monitoring absorbance at 329 nm (Kratos SF769Z). To keep the concentration in the final solution as high as possible, only the center cut of the eluting peak was collected. The resulting solution had an absorption coefficient of $\sim 5\ cm^{-1}$ at 329 nm.

The electric field was created between two copper plates of area 0.6 cm $\times$ 1.2 cm held at 0.22 cm separation by Delron spacers. The sample in a melting point capillary capped with Teflon tape was held by friction in the center of the electrode assembly. In an experiment this electrode assembly, mounted at the end of a thin stainless steel tube, was slowly introduced (over ~ 10 min) into the liquid He reservoir of a home-built optical cryostat. Once the sample was in place, the vapor pressure over the liquid He in which it was immersed was reduced to ~ 1 Torr with a pumping system consisting of a Leybold Heraeus AM 90 SZ4 backed WS250 Rootes pump.

The optical arrangement for these experiments is shown in Fig. 1. The exciting light propagated at right angles to the applied electric field and parallel to the axis of the signal photomultiplier. In most experiments, the excitation light was polarized either parallel or perpendicular to the applied electric field and there were no polarization sensitive elements in the signal channel. The photomultipliers in the sample and reference channels were identical (RCA 1P28) and were run at the same voltage. The signal photomultiplier viewed the sample through a sharp cut off filter (Schott KV389) which was mounted against the cryostat window. The reference photomultiplier looked at a small fraction of the irradiating beam through a solar blind filter (Corning 9863), a 2 o.d. neutral density filter (Esco) and whatever additional neutral density filters were required to keep the signal and reference photomultiplier anode currents roughly equal. The photomultiplier anode currents were read with two electrometers (Kiethley 610B and 610C). The analog outputs from the electrometers were integrated by a Hewlett Packard Model 310 computer which also collected laser wavelengths and scan parameters from the Apple IIe microcomputer that is part of the Coherent 699 Autoscan system.

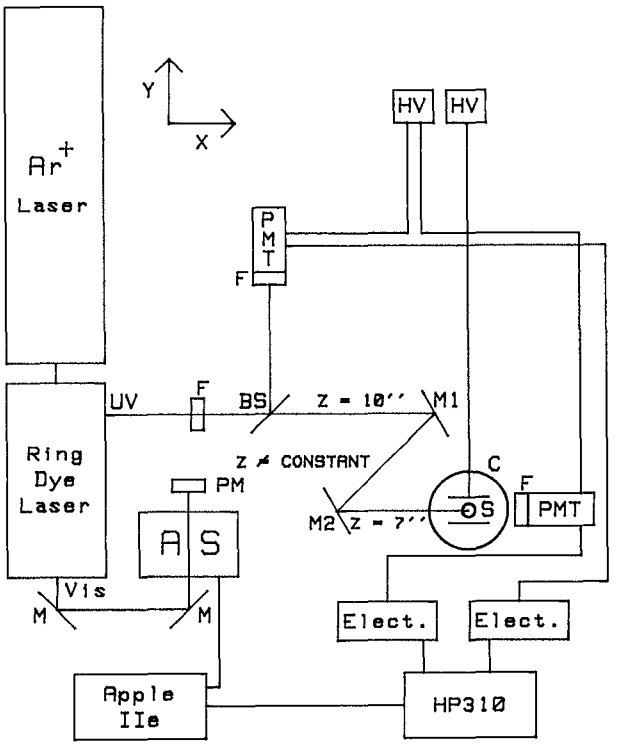

FIG. 1. Experimental arrangement for the hole burning studies. F=filter, BS=beam splitter, C=cryostat, S=sample and Stark cell, Vis =fundamental output of the ring laser, UV=second harmonic of the ring laser fundamental, M=mirror, HV=high voltage power supply, PMT =photomultiplier tube, AS=autoscan, and PM=power meter.

The excitation source for these experiments was an actively stabilized single frequency ring dye laser (Coherent 699-29) with optics coated for 630–810 nm. The laser dye was LD688 (Exciton) dissolved in a 90:10 by volume mixture of benzyl alcohol and glycerin maintained at 5 °C by a standard cooler (Nestlab CFT33). Stability and output power were enhanced by replacing the original dye nozzle with a polished stainless steel nozzle that gives an interferometrically flat jet at pressures up to 90 psi (Radiant Dye). The ultraviolet (UV) output was generated by an intracavity $LiIO_3$ doubling crystal Brewster cut for operation 318–350 nm (Coherent 7500-02). Because we only needed low UV powers and wanted to preserve the function of the scanning electronics (Coherent Autoscan) we used the normal output coupler ($\sim 3\%$ transmission) rather than the 0.1% transmission output coupler that would optimize UV output.

In a typical experiment a persistent photochemical hole was burned by setting the laser to a wavelength within the inhomogeneous width of the zero-phonon component of the 1 $^1A_g \rightarrow 2\ ^1A_g$ 0–0 band, optimizing the UV output, and then allowing the unattenuated beam to irradiate the sample for 15 s. The laser output was then reduced by a

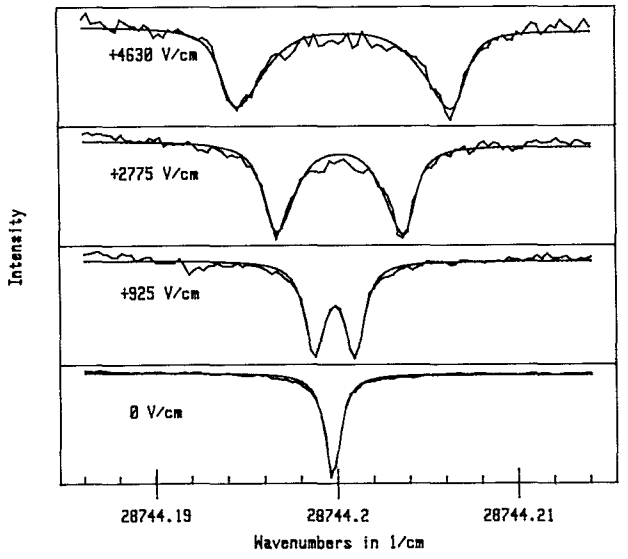

FIG. 2. Splitting of a persistent photochemical hole in the octatetraene in *n*-hexane produced by a static electric field. The hole was burned in zero field and then scanned at the different field strengths indicated on the four curves. The burning and scanning laser was polarized parallel to the static field in all scans. The noisy curves are the measured data, the smooth lines are the profiles calculated with the model described in Sec. IV A.

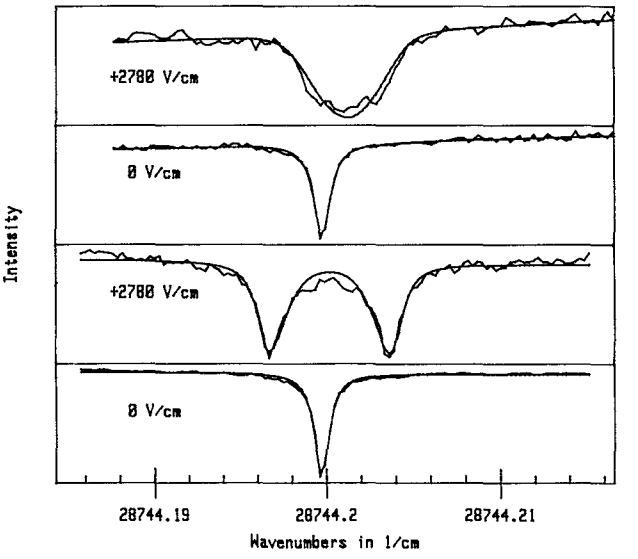

FIG. 3. Polarization dependence of the electric field induced splitting for the octatetraene *n*-hexane system. For the lower two curves the burning and scanning light was polarized parallel to the applied field, for the upper two curves the burning and scanning light was polarized perpendicular to the applied field. The noisy curves are the measured data, the smooth lines are the profiles calculated by the model described in Sec. IV A.

factor of 10 with a 1 o.d. neutral density filter and the holes scanned over a 2 GHz range centered on the wavelength at which the hole was burned at a rate of 20 MHz/s. Scans were repeated at different applied voltages. Periodically, the zero field hole profile was remeasured in order to have a quantitative estimate for the long time frequency drift of the laser and to determine the extent to which the original profile had been altered by repeated scanning.

III. RESULTS

Over 100 scans of photochemical hole profiles in the $1\ ^1A_g \rightarrow 2\ ^1A_g$ 0–0 for a variety of positions in the inhomogeneous profile, applied field strength and angle between the laser polarization and the applied electric field were collected. Figure 2 shows the effect of electric fields up to 4.6 kV/cm on the fluorescence excitation profile of a photochemical hole burnt into the $1\ ^1A_g \rightarrow 2\ ^1A_g$ 0–0 transition of *trans,trans*-octatetraene in randomly oriented microcrystals of *n*-hexane. For the data in Fig. 2 the hole was burned and scanned with the laser polarized parallel to the applied electric field. Because the sample consists of nonpolar molecules with a well defined orientation in the host lattice, one might have expected a second order shift which, given the relatively small magnitude of the applied field and the fact that it is randomly oriented in the octatetraene axis system, would have just caused the hole to slightly broaden to lower energy with the application of an external electric field. (As seen, for example, for tetracene and pentacene in *p*-terphenyl.[19]) Instead, the observed behavior is superficially similar to results reported for chlorin in the polar polymer poly(vinyl butyral) by Meixner, Renn, Bucher, and Wild.[6] To within our current level of precision, the hole profile splits and broadens symmetrically with increasing applied field. While we have used a more elaborate semi-classical model for the hole profiles (described in detail in Sec. IV A), the hole profiles in Fig. 2 can be well fit by the sum of two Lorentzians plus a slanting base line. To within experimental error, the splittings extracted from this kind of analysis depend linearly on the magnitude of the applied field.

The electric field induced change in hole profile depends strongly on the polarization of the laser relative to the applied dc field. Figure 3 compares the electric field induced splitting observed when the burning and scanning laser is polarized parallel to the applied electric field to that obtained when the burning and scanning laser is polarized perpendicular to the applied electric field. When the burning and scanning laser polarization is perpendicular to the applied field the hole does not split, but broadens and becomes more rectangular. This is superficially similar to the results on chlorin and Zn–tetrabenzoporphin reported by Kador, Haarer, and Personov.[7]

The polarization dependence of the electric field perturbed hole profile that is seen in Figs. 2 and 3 (splitting when the light was polarized parallel to the applied field and broadening when the light was polarized perpendicular to the applied field) was generally observed. In the cases where the laser was polarized parallel to the applied field we did observe occasional variation of the observed splitting with sample or with position on a given sample. We believe that this was a consequence of depolarization of the incident laser beam by multiple scattering, an effect which is quite sensitive to details of the crystallite size distribution in the polycrystalline samples. However, the striking dependence of the electric field perturbed hole pro-

file on laser polarization indicates that it is appropriate to interpret these results in terms of an ensemble of randomly oriented microcrystals for which the applied electric field and the laser polarization are well defined quantities. This receives further support from the quantitative success of the model described below.

IV. DISCUSSION AND ANALYSIS

Because both the guest octatetraene and host *n*-hexane are intrinsically nonpolar molecules, the observation of the large splittings seen in Fig. 2 and the linear dependence of those splittings on electric field strength was to us at first surprising. This large first order splitting where a small second order effect would have been expected indicates two things, first, the *n*-hexane host crystal has induced a significant ($\sim$0.1 D) permanent dipole moment difference between the 1 ^1A_g and 2 ^1A_g states and, second, every octatetraene molecule in the ensemble has nearly the same induced dipole moment difference.

There are two reasons why it is not reasonable to postulate that this permanent dipole moment difference results from a lattice induced geometrical distortion of the octatetraene from a centrosymmetric geometry. First, the octatetraene is not expected to have a permanent dipole moment for any nearly planar geometry because of the charge neutrality that is expected for the repeat units of a hydrocarbon polyene chain. Second, a significantly distorted structure is inconsistent with the fact that the ground and excited state vibrational frequencies for octatetraene in *n*-hexane are nearly identical to those observed for octatetraene in *n*-octane where the molecule is certainly *trans* planar.[20] On the other hand, the relatively close proximity of the 2 ^1A_g and 1 ^1B_u excited states and the fact that they are connected by the electric dipole moment operator naturally leads to the idea that this effective difference in permanent dipole moment is a consequence of the polarization of the octatetraene molecule by a local electric field. This is supported by experiments such as the one shown in Fig. 4 which demonstrate that the observed splitting is consistent with the effective electric field at the octatetraene molecule being the vector sum of the applied field and a well defined internal field. Thus, to explain our observations we have invoked a simple semiclassical model for the electrostatic interaction between solvent and solute molecules. In this model, the guest molecule sees the vector sum of the externally applied field and an internal field generated by the surrounding solvent molecules. With only two parameters, the 2 $^1A_g \rightarrow 1\ ^1B_u$ transition dipole and the component of the internal field along this dipole, this model quantitatively accounts for all our measured profiles. Further, the magnitude of the internal field determined by fitting the field dependence of the measured profiles for different polarizations of the burning and scanning light is consistent with the field calculated for a particular two-molecule vacancy in the *n*-hexane crystal by summing the C–H bond dipole fields over the lattice.

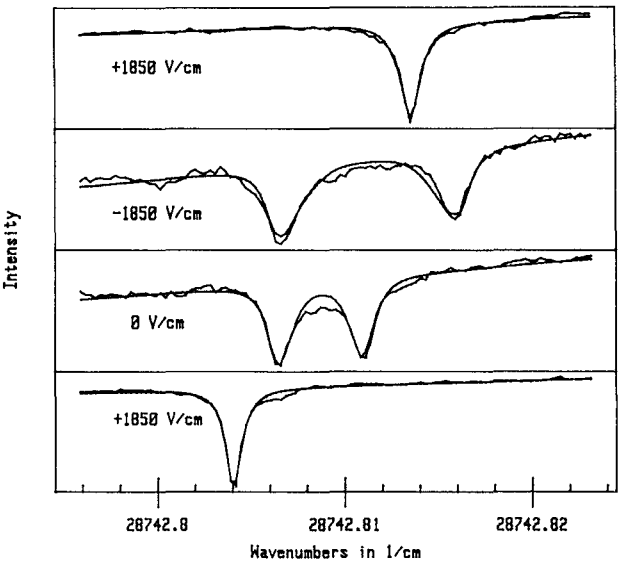

FIG. 4. Vector addition of internal and external electric fields. The bottom panel shows a photochemical hole burned in the presence of an 1850 V/cm applied electric field. When the field is turned off, the hole splits as shown in the panel second from the bottom. The panel second from the top shows that, if the 1850 V/cm field is restored but with the opposite sign, the splitting doubles. The upper panel shows the recovery of the original unsplit hole when the sense of the 1850 V/cm applied field is the same as when the hole was originally burned. These four traces were taken sequentially in time from bottom to top, light was polarized parallel to the applied field. The noisy curves are the measured data, the smooth lines the profiles calculated with the model described in the text. As is apparent, the laser was slowly drifting to higher frequency in this series of scans.

A. The model

The Hamiltonian for octatetraene in an external electric field $\mathbf{E}$ may be written

$$H = H_0 + \mathbf{E}\cdot\mu, \tag{1}$$

where the eigenfunctions of H_0 are the eigenstates of octatetraene, μ is the dipole moment operator, and $\mathbf{E}\cdot\mu$ describes the perturbation of the octatetraene eigenstates by the electric field at the octatetraene molecule. Writing this Hamiltonian in the purely electronic basis 1 ^1A_g, 2 ^1A_g, and 1 ^1B_u gives the 3×3 matrix

$$H = \begin{array}{c} \begin{matrix} 1\ ^1A_g & 2\ ^1A_g & 1\ ^1B_u \end{matrix} \\ \begin{bmatrix} 0 & 0 & \mathbf{E}\cdot\mu_1 \\ 0 & E(2\ ^1A_g) & \mathbf{E}\cdot\mu_2 \\ \mathbf{E}\cdot\mu_1 & \mathbf{E}\cdot\mu_2 & E(1\ ^1B_u) \end{bmatrix} \end{array} \begin{matrix} 1\ ^1A_g \\ 2\ ^1A_g \\ 1\ ^1B_u \end{matrix}, \tag{2}$$

where $E(2\ ^1A_g)/hc = 28\,745\ \text{cm}^{-1}$ and $E(1\ ^1B_u)/hc = 32\,245\ \text{cm}^{-1}$ are the measured 0–0 excitation energies, μ_1 is the 1 $^1A_g \rightarrow 1\ ^1B_u$ transition dipole and μ_2 is the 2 $^1A_g \rightarrow 1\ ^1B_u$ transition dipole. Because the energy separation between the 2 ^1A_g and 1 ^1B_u levels is an order of magnitude smaller than the separation between the 1 ^1A_g and 1 ^1B_u levels, the effect of the electric field $\mathbf{E}$ for the field strengths used in these experiments is reasonably described

by considering only the mixing of the 2 ^1A_g and 1 ^1B_u levels [although, our final analysis used the three-level Hamiltonian of Eq. (2)].

The electric field at the molecule is assumed to have two contributions, a well defined internal field $\mathbf{E}_0$ and the field $\mathbf{E}_s$ generated by the externally applied field. $\mathbf{E}_s$ may be approximated by

$$\mathbf{E}_s=\frac{n^2+2}{3}\mathbf{E}_{\text{lab}}, \tag{3}$$

where $\mathbf{E}_{\text{lab}}$ is the laboratory field (voltage impressed on the parallel plates divided by their separation) and ϵ, the dielectric constant for n-hexane, has been approximated by the square of the refractive index n.[21] Clearly, what is most important are the projections of the fields $\mathbf{E}_0$ and $\mathbf{E}_s$ on the transition dipole μ_2 which we write as E_0 and E_s, respectively. Since the sample consists of randomly oriented crystallites, E_s for the experimental ensemble will be random over a sphere. That is, a given molecule in the ensemble will see the field magnitude $E=E_0+E_s\cos\theta$.

To calculate the hole profile for a given applied field in the two-level approximation, the 2×2 matrix

$$H=\begin{bmatrix} 0 & (E_0+E_s\cos\theta)\mu_2 \\ (E_0+E_s\cos\theta)\mu_2 & 3500\ \text{cm}^{-1}\times hc \end{bmatrix} \tag{4}$$

is diagonalized for a given θ, the lower eigenvalue is weighted as described in the next paragraph, convolved with a Lorentzian, and accumulated. This is repeated for θ values running from 0 to π at intervals of 0.01π. Equation (4) may be viewed as a special case of the three-level Hamiltonian of Eq. (2). Our final analysis used the three-level Hamiltonian with the projection of the 1 ^1A_g to 1 ^1B_u transition dipole fixed to various values.

The weight for the eigenvalue computed for a given value of θ is the probability that the molecule at that θ underwent photochemistry during the intense irradiation times the probability that it is excited in the fluorescence excitation readout times the probability of that θ. The probabilities of the excitation events are proportional to the squared dot products of the electric vector of the light with the 1 $^1A_g \rightarrow 2\ ^1A_g$ transition dipole which vibronic coupling arguments would say is parallel to the 1 $^1A_g \rightarrow 1\ ^1B_u$ transition dipole μ_1. At this level of treatment we may also assume that the 2 $^1A_g \rightarrow 1\ ^1B_u$ transition dipole μ_2 in these linear chain molecules is nearly parallel to μ_1.

Choosing laboratory axes such that the z-axis is parallel to the dc electric field and the y-axis is parallel to the propagation direction of the light the applied yield $\mathbf{E}_s$, the polarization vector for the light $\hat{\mathbf{e}}$, and unit vectors along the transition dipoles μ_1 and μ_2 are written

$$\mathbf{E}_s=E_s\begin{bmatrix}0\\0\\1\end{bmatrix}, \tag{5}$$

$$\hat{\mathbf{e}}=\begin{bmatrix}\sin\theta^\circ\\0\\\cos\theta^\circ\end{bmatrix}, \tag{6}$$

and

$$\hat{\mu}_1=\hat{\mu}_2=\begin{bmatrix}\sin\theta\cos\phi\\\sin\theta\sin\phi\\\cos\theta\end{bmatrix}. \tag{7}$$

The excitation intensity is proportional to

$$(\hat{\mathbf{e}}\cdot\hat{\mu}_2)^2=(\sin\theta^\circ\sin\theta\cos\phi+\cos\theta^\circ\cos\theta)^2. \tag{8}$$

In our experiments the laser polarization during photochemical hole burning was the same as during the fluorescence excitation readout so the weighting factor for a given θ, $W(\theta)$, is the product of relative probabilities for hole burning and subsequent readout averaged over ϕ and multiplied by $\sin\theta d\theta$,

$$\begin{aligned}W(\theta)d\theta=(&\tfrac{3}{8}\sin^4\theta^\circ\sin^4\theta\\&+3\sin^2\theta^\circ\cos^2\theta^\circ\sin^2\theta\cos^2\theta\\&+\cos^4\theta^\circ\cos^4\theta)\sin\theta d\theta.\end{aligned} \tag{9}$$

Since our polycrystalline samples are not optically homogeneous, the excitation light is depolarized as it propagates into the sample. In the limit of total depolarization, the weight given in Eq. (9) should be integrated over θ°. Integration over the full range of θ° is clearly inappropriate since, as is clearly seen in Fig. 3, the hole profiles observed for $\theta^\circ=0$ and $\theta^\circ=\pi/2$ are completely different. Moreover, the data for a given θ° in a large number of different runs using different samples on different days and burning different positions in the inhomogeneous profile were very similar. Given this and the fact that a number of approximations have already been made (simple Lorentz scaling for computing the internal field, parallel transition dipoles, three state model) the neglect of depolarization effects seems reasonable. This is buttressed by the ability of this simple model to quantitatively reproduce 20 experimental scans (over 2100 data points with $\theta^\circ=0$ or $\pi/2$) to within our present signal to noise ratio. It is clearly possible to go beyond the approximations made in the present analysis and extract much more detailed information on both the 1 $^1A_g \rightarrow 1\ ^1B_u$ and 2 $^1A_g \rightarrow 1\ ^1B_u$ transition dipoles. This will be important for the analysis of much more extensive data on single crystal samples which we are currently trying to obtain.

B. The fits

The data set for analysis consisted of 20 scans of photochemical hole profiles in the presence of an applied electric field. These scans were taken for seven different samples; data on a given sample were measured at a number of different field strengths. The burning and scanning laser was polarized parallel to the applied field for roughly two thirds of the scans, perpendicular for the rest. Each of these scans was bracketed by scans taken at zero applied field which were used to fix the width of the Lorentzian used in the convolution described in Sec. IV A to verify that the readout process had not modified the hole profile, and to monitor long term laser drift. At a given μ_1 (zero for the two-level limit), a single μ_2, E_0 pair quantitatively fit all 20 scans within their signal to noise ratio. The level

TABLE I. Molecular field in 10^6 V/cm obtained by fitting hole profile as a function of electric field strength for different values of the $1\ ^1A_g$–$1\ ^1B_u$ and $2\ ^1A_g$–$1\ ^1B_u$ transition dipoles.

		$1\ ^1A_g \rightarrow 1\ ^1B_u$ Dipole in debye			
		7.5	8.0	8.5	9.0
$2\ ^1A_g \rightarrow 1\ ^1B_u$ Dipole in debye	2.2	4.56	2.82	1.98	1.51
	2.0	2.83	2.03	1.56	1.25
	1.8	2.09	1.62	1.30	1.08

of agreement between the measured and calculated profiles is shown in Figs. 2–4. As would be expected, the parameters μ_2 and E_0 are strongly correlated over the relatively small range of applied electric field strength that we have so far covered. Their values also depend on the value chosen for μ_1, the magnitude of the $1\ ^1A_g$ to $1\ ^1B_u$ transition dipole, although this dependence is relatively weak. Sets of parameters that quantitatively reproduce the observed profiles are summarized in Table I and the dependence of the E_0 local field parameter on the values of the two transition dipoles μ_1 and μ_2 is depicted graphically in Fig. 5. While the ability of these initial experiments to simultaneously determine precise values for the magnitudes of the internal field and the $2\ ^1A_g$ to $1\ ^1B_u$ transition dipole is limited, the allowable values of these quantities may have is rather precisely fixed. If we set the transition dipole magnitudes μ_1 and μ_2 to the values obtained from theory by Soos and Ramasesha[16] (8.7 and 2.1 D, respectively), the magnitude of the internal field E_0 is determined by these experiments to be 1.6×10^6 V/cm. If we assume that the actual effective transition dipole magnitudes differ from the values calculated by Soos and Ramasesha by no more than 20% then $1\times10^6\ \text{V/cm} < E_0 < 8\times10^6$ V/cm. In the next section we consider how such a large field may be present in an ordered crystal of nonpolar molecules.

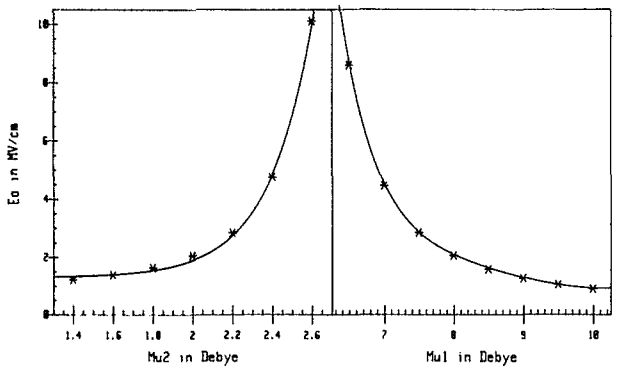

FIG. 5. Molecular field obtained by fitting hole profile as a function of electric field strength for different values of the $1\ ^1A_g$–$1\ ^1B_u$ and $1\ ^1A_g$–$1\ ^1B_u$ transition dipoles.

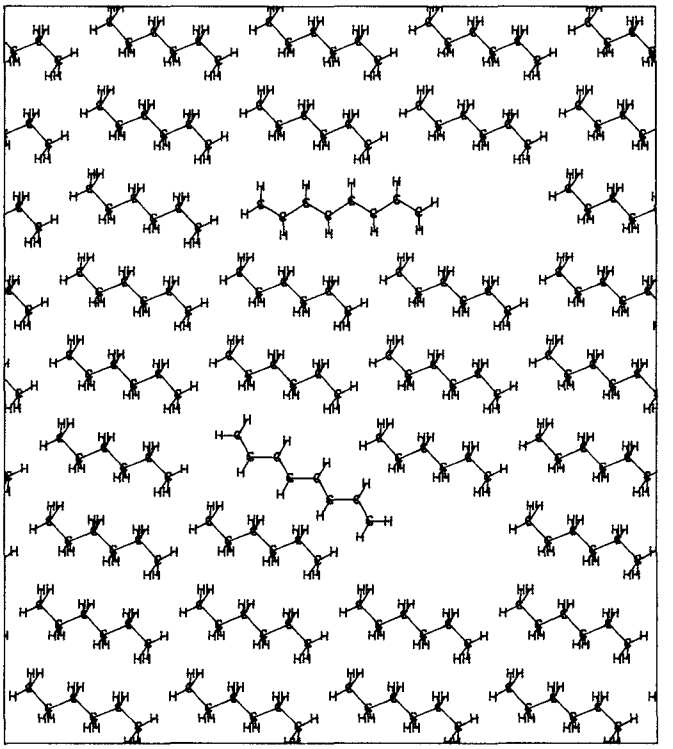

FIG. 6. A *bc* plane projection of the *n*-hexane crystal structure showing the two-molecule defect sites that can accommodate octatetraene. The projection of the crystal field on the octatetraene chain axis for the upper site (vacancies related by a [0,0,1] translation) is significantly smaller than for the lower site (vacancies related by a [0,1,1] translation).

C. The site

The fact that the absorption and fluorescence spectra have narrow inhomogeneous linewidths (HWHM ~ 2 cm^{-1}) and that the vibronic band profile exhibits a highly structured phonon side band establishes that the octatetraene molecules sit in a well defined site in a crystallographically ordered *n*-hexane lattice An octatetraene molecule is significantly longer than an *n*-hexane molecule; from x-ray crystallographic data we know that the molecular volumes of octatetraene and *n*-hexane are 174 (Ref. 22) and 161 Å^3 (Ref. 23), respectively. Because of this disparity in molecular sizes, a simple structure where one octatetraene molecule replaces one *n*-hexane molecule can be ruled out. However, a site generated by the removal of two adjacent *n*-hexane molecules from the lattice easily accommodates an octatetraene molecule. There are three possibilities for this kind of vacancy. The two missing *n*-hexane molecules can be related to each other by translation along the *b*-axis (010) the *c*-axis (001) or along the *bc* diagonal (011). Of these three possibilities, only the second and third lead to an elongated vacancy with a cross section that is close to that of an octatetraene molecule. These vacancies are shown in Fig. 6.

Now, we consider the source of the local electric field. Although the *n*-alkanes have no overall dipole moment, the C–H bonds are actually quite polar. The commonly used value of 0.4 D with the hydrogen positively charged is

TABLE II. Electric fields in the two molecule vacancies in *n*-hexane that are shown in Fig. 2 (*bc* projection). Fields were computed for the carbon atom coordinates of the left-most eight carbons of the missing pair of *n*-hexane molecules by summing the contributions from all C–H bond dipoles (0.4 D).

	b site E_0 (10^6 V/cm)			*bc* site E_0 (10^6 V/cm)		
Atom	*b* component	*c* component	long axis projection	*b* component	*c* component	long axis projection
1	6.60	5.88	5.88	6.84	5.49	8.72
2	5.19	1.47	1.47	5.76	0.99	4.77
3	2.07	2.13	2.13	2.73	1.14	2.73
4	−2.19	−0.18	−0.18	−0.54	−1.29	−1.29
5	−5.58	1.71	1.71	−3.33	−2.01	−3.78
6	−9.18	−1.59	−1.59	−1.17	−6.75	−5.61
7	9.18	1.59	1.59	1.17	6.75	5.61
8	5.58	−1.71	−1.71	3.33	2.01	3.78

based on an analysis of experimental data.[24] Since the C–H bond polarities derived from quantum mechanical calculations tend to be at least a factor of 2 larger,[25] we can safely assume that 0.4 D should be viewed as a lower bound. An estimate of the magnitude of the electric field at any point in the *n*-hexane sites shown in Fig. 6 may be obtained by superposing the fields from all of the C–H bond dipoles in the surrounding lattice. The fact that a dipole field falls off with distance cubed insures the rapid convergence of this sum. In order to get an indication of the nature of the local electrical field at the octatetraene guest molecule we have carried out this classical electric field calculation for points in the site at the coordinates of the leftmost eight carbon atoms of the pair of missing *n*-hexane molecules. The electric fields calculated for these positions are summarized in Table II and Fig. 7. It is clear that the orientations of the fields for the *b* and *bc* diagonal sites are strikingly different and that the field projections for the *bc* diagonal site are much more compatible with the E_0 value derived from these experiments.

Finally, it is interesting to see if variation of this large local electric field makes a significant contribution to the inhomogeneous broadening. Figure 8 summarizes the dependence of the magnitude of the splitting produced by the application of a 1850 V/cm field on position in the inhomogeneous profile. Within the limitations set by our current signal to noise ratio it appears that the internal field is constant over the inhomogeneous band, that is, the disorder that is responsible for the inhomogeneous broadening has little effect on the local electrostatic environment of the guest molecules.

Of course, this low level of analysis can be vastly improved by replacing the very crude approximation that interaction energies may be described by the dot product of a point dipole with a homogeneous electric field by a more sophisticated model. This will be justified when data that cover a much broader range of electric field strengths are obtained for single crystal samples. These initial experiments clearly show that such measurements will provide an extremely powerful method that cannot only directly measure such important aspects of linear polyene electronic structure as off-diagonal dipole moment expectation values, but give us a method for directly characterizing electrostatic properties on a molecular scale.

V. CONCLUSIONS

Photoisomerization of octatetraene guest molecules in low temperature *n*-hexane host crystals with a single frequency laser produces extremely narrow persistent holes in the inhomogeneously broadened zero-phonon component of the 1 $^1A_g \rightarrow 2\ ^1A_g$ 0–0 band. The application of a 1 kV/cm external electric field splits this hole profile when the burning and scanning laser is polarized parallel to the applied field and broadens it when the burning and scanning laser is polarized perpendicular to the applied field. The hole profiles measured under a wide range of conditions (angle

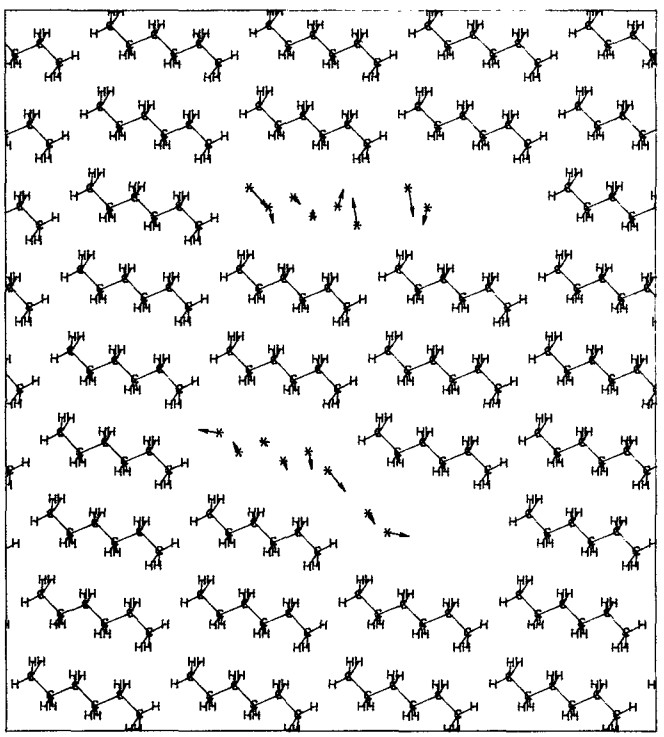

FIG. 7. Internal electric fields for the two different two-molecule vacancies in the *n*-hexane crystal structure that could accommodate an octatetraene guest molecule. Values for the fields at the coordinates of the carbon atoms of the missing molecules were computed by superposing the dipole fields from all C–H bonds in the lattice. The *b* vacancy is shown in the left panel, the *bc* vacancy in the right panel.

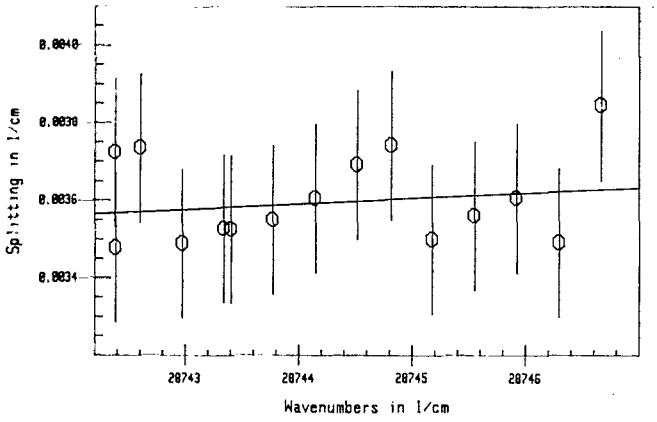

FIG. 8. Electric field induced splitting of a persistent photochemical hole in the zero-phonon component of the 1 $^1A_g \rightarrow 2\ ^1A_g$ 0–0 band of octatetraene in polycrystalline *n*-hexane as a function of position in the inhomogeneous profile.

between the laser polarization and the static field 0 or $\pi/2$, static field strength 0–3 kV/cm) are all quantitatively fit by a semiclassical three-level model that includes a $1\text{–}8\times10^6$ V/cm internal electric field that is intrinsic to the octatetraene site. These experiments open a powerful method for obtaining a much deeper characterization of linear polyene electronic structure and for determining the electrostatic properties of molecular environments.

[1] J. H. Meyling, W. H. Hesslink, and D. A. Wiersma, Chem. Phys. **17**, 353 (1976).
[2] A. I. M. Dicker, L. W. Johnson, M. Noort, and J. H. van der Waals, Chem. Phys. Lett. **94**, 14 (1983).
[3] U. Bogner, P. Shatz, and M. Maier, Chem. Phys. Lett. **141**, 31 (1983).
[4] F. A. Burkhalter, G. W. Suter, U. P. Wild, V. D. Samoilenko, N. V. Rasumova, and R. I. Personov, Chem. Phys. Lett. **94**, 483 (1984).
[5] U. P. Wild, S. E. Bucher, and F. A. Burkhalter, Appl. Opt. **24**, 1526 (1985).
[6] A. J. Meixner, A. Renn, S. E. Bucher, and U. P. Wild, J. Phys. Chem. **90**, 6777 (1986).
[7] L. Kador, D. Haarer, and R. Personov, J. Chem. Phys. **86**, 5300 (1986).
[8] L. W. Johnson, M. D. Murphy, C. Pope, M. Forsetti, and J. R. Lombardi, J. Chem. Phys. **86**, 4335 (1987).
[9] L. Kador and D. Haarer, J. Appl. Phys. **62**, 4226 (1987).
[10] J. Gerblinger, U. Bogner, and M. Maier, Chem. Phys. Lett. **102**, 267 (1983).
[11] W. Gu and D. M. Hanson, J. Chem. Phys. **89**, 2615 (1988).
[12] L. Kador, S. Jahn, D. Haarer, and R. Silbey, Phys. Rev. B **41**, 12 215 (1990).
[13] M. Orrit, J. Bernard, A. Mouhsen, H. Talon, D. Mobius, and R. I. Personov, Chem. Phys. Lett. **179**, 232 (1991).
[14] D. Baeriswyl, D. K. Campbell, and S. Mazumdar in *Conducting Polymers*, edited by H. Kiess (Springer, Berlin, 1990).
[15] B. E. Kohler, J. Chem. Phys. **93**, 5838 (1990).
[16] Z. G. Soos and S. Ramasesha, J. Chem. Phys. **90**, 1067 (1989).
[17] G. Adamson, G. Gradl, and B. E. Kohler, J. Chem. Phys. **90**, 3038 (1989).
[18] C. Spangler and D. A. Little, J. Chem. Soc. Perkins Trans. **1**, 2379 (1982).
[19] J. H. Meyling and D. A. Wiersma, Chem. Phys. Lett. **20**, 383 (1973).
[20] M. F. Granville, G. R. Holtom, and B. E. Kohler, J. Chem. Phys. **72**, 4671 (1980).
[21] For the refractive index of crystalline *n*-hexane we used 1.527, derived from the handbook value for the 20 °C liquid $n_D = 1.375\ 06$ by assuming that $(n^2-1)/(n^2+2)$ is proportional to density. The density of crystalline *n*-hexane (0.887 g cm^{-3}) was computed from the x-ray data of Ref. 23.
[22] R. H. Baughman, B. E. Kohler, I. J. Levy, and C. Spangler, Syn. Met. **11**, 37 (1985).
[23] N. Norman and H. Mathisen, Acta Chem. Scand. **15**, 1755 (1961).
[24] For example, see C. P. Smyth, *Dielectric Behavior and Structure* (McGraw–Hill, New York, 1955), pp. 243-244.
[25] A Gaussian-90 RHF 3-21G *ab initio* calculation of the electronic structure of *n*-hexane predicts C–H bond dipole moments to be 1.05 D, with the hydrogen atom positive; Jörg Woehl (private communication).